Available online at www.sciencedirect.com
SCIENCE DIRECT®
International Journal of Heat and Mass Transfer 48 (2005) 2278–2289
International Journal of HEAT and MASS TRANSFER
www.elsevier.com/locate/ijhmt

Weakly non linear convection in a shallow horizontal cavity under uniform crossed heat fluxes

Michel Prud'homme *, Habiba Bougherara

Department of Mechanical Engineering, École Polytechnique de Montréal, C.P. 6079, Succ. Centre-ville, Montréal, QC, Canada H3C 3A7

Received 7 April 2004; received in revised form 5 November 2004
Available online 26 February 2005

Abstract

A weakly nonlinear stability analysis is developed for the unicellular natural convection pattern in a horizontal fluid layer heated by uniform crossed heat fluxes applied on the horizontal and vertical walls, the remaining walls being adiabatic. The critical Rayleigh number is determined, for different Prandtl numbers and heat flux ratios, from the analytical parallel approximation for the single cell flow. For the range of parameters considered, stable, supercritical bifurcations occur solely for longitudinal disturbances with three velocity components. Depending on the value of *Pr* and the heat flux ratio, the instability is oscillating and hydrodynamic at small *Pr* and thermal and steady for larger *P*r. Computations of the Landau coefficients for the two interacting modes reveal that the hydrodynamic mode is the only stable mode at the codimension points.

1. Introduction

It is now well established in the literature on natural convection that the unicellular base flow encountered in a rectangular enclosure at low Rayleigh numbers undergoes a series of bifurcations as the Rayleigh number increases, in porous as well as in fluid medium. For isothermal boundary conditions imposed on the top and bottom walls, in a porous medium, Riley and Winters [1] reported that the unicellular pattern is the preferred form of primary flow in two dimensions for small enclosure aspect ratios. If the problem is extended to three dimensions, it is found that the boundary conditions imposed on the side walls do play a very important role in setting the value of the critical Rayleigh number and the type of modal configuration, as reported by Murphy [2] and Wang et al. [3], among others.

When heating the enclosure by applying a constant heat flux on the horizontal walls is considered, unicellular flow patterns may also be obtained at low Rayleigh numbers, as reported by Bejan [4], for a thin vertical porous cavity insulated on the neighboring sides. Later, Vasseur et al. [5] and Sen et al. [6] analysed the stability of the unicellular pattern for an inclined shallow porous cavity subjected to a constant flux on the facing walls. The aforementioned uniform flux condition can be encountered when considering a finite conductivity slab adjacent to a porous layer as discussed by Kimura and Pop [7] or in the study of electrochemical systems, as reported by Bark et al. [8].

* Corresponding author. Tel.: +1 514 340 4711; fax: +1 514 340 5917.
E-mail address: miprud@meca.polymtl.ca (M. Prud'homme).

0017-9310/$ - see front matter © 2005 Elsevier Ltd. All rights reserved.
doi:10.1016/j.ijheatmasstransfer.2004.11.022

Nomenclature

a	aspect ratio
A	amplitude
$\mathbf{A}$	matrix operator
$\mathbf{B}$	constant matrix
D	derivative
d	distance between the walls
E	complex exponential
g	gravity
H	differential operator
k	horizontal wavenumber
L	differential operator
$\mathbf{L}$	matrix operator
l	transverse wavenumber
N	number of grid points
p	pressure
Pr	Prandtl number
Q	transverse heat flux
q	heat flux ratio
Ra	Rayleigh number
t	time
T	temperature
$\mathbf{u}$	velocity vector
u, v, w	velocity components
x, y, z	coordinates
$\mathbf{x}$, $\mathbf{z}$	unit vectors

Greek symbols

α	horizontal temperature gradient
β	direction of propagation
θ	base flow temperature profile
σ	complex amplification rate
ψ	base flow stream function

Superscripts

$\dagger$	adjoint quantity, 3-D
$\wedge$	disturbance quantity, 1-D
$*$	complex conjugate

Subscripts

c	critical value
H	hydrodynamic
i	imaginary part
r	real part
T	thermal
0	reference value

Other symbols

D/Dt	material derivative
$\|\|$	modulus
∇	gradient
∇^2	Laplacian

Kimura et al. [9] considered the stability problem in three dimensions in a shallow horizontal porous layer insulated on the vertical boundaries and heated by a constant heat flux applied from below. Their conclusions were that the steady parallel base flow is linearly stable to longitudinal and transverse disturbances at first for small Rayleigh numbers and that a Hopf bifurcation occurs first for longitudinal disturbances, at some critical Rayleigh number for a given aspect ratio, leading to oscillating instabilities. In a slightly different context, Nield [10] also showed that similar instability regimes could be obtained in a shallow porous layer submitted to an oblique temperature gradient, by varying the vertical to lateral temperature gradient ratio.

For a fluid medium, Bergholz [11] determined that the instability in a vertical cavity with a fixed temperature difference on the sides is either of hydrodynamic or thermal origin depending on the Prandtl Number, and that transition from stationary to oscillatory instability modes happens with increasing thermal stratification at small Prandtl numbers, and the other way around at large Prandtl numbers.

Although unicellular convection sustained by a uniform heat flux applied on some parts of the boundary can be encountered in many types of enclosure configurations, nearly adiabatic conditions on the rest of the boundary do not always occur in practice. Since the instability regime of the flow for isothermal heating is so sensitive to the sidewall thermal conditions, it is worthwhile to extend the previous studies by undertaking a weakly non linear stability analysis of unicellular convection for a horizontal fluid layer heated by crossed uniform heat fluxes of different magnitudes. The critical Rayleigh number will be determined for a range of Prandtl numbers and heat flux ratios q by solving the linear equations. The Landau coefficients will be computed for the different instability modes and bimodal stability considered at the codimension points.

2. Problem definition

Let us consider a shallow horizontal cavity extending widely along the x and z directions as in Fig. 1. The stability of natural convection flow inside the enclosure is examined for adiabatic conditions in the z-direction and uniform heat fluxes on the remaining walls, as sketched. It is assumed from the beginning that the temperature differences involved in the problem are small enough to allow us to make the standard Boussinesq

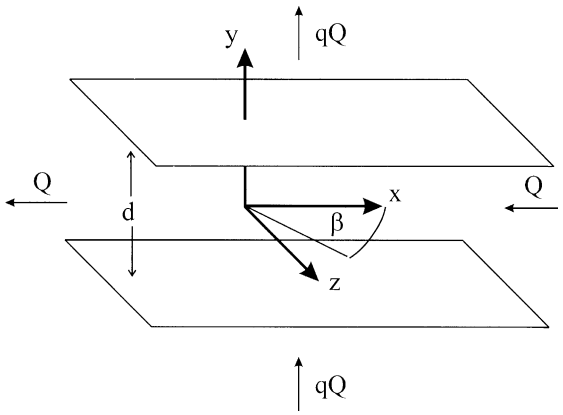

Fig. 1. Geometry and coordinate system.

approximations [12]. When convection occurs within a newtonian fluid of constant kinematic viscosity ν, thermal diffusivity α_T and coefficient of thermal expansion β_T, it is convenient to scale length, temperature, velocity and time with reference to

$$d, \Delta T = \frac{Qd}{k_T}, \frac{\alpha_T}{d}, \frac{d^2}{\alpha_T} \tag{1}$$

where all properties are evaluated at some reference temperature T_0. Based on the Boussinesq approximation $\rho = \rho_0[1 - \beta_T(T - T_0)]$ in the expression for the buoyancy force, the set of governing equations for the dimensionless problem become

$$\nabla \cdot \mathbf{u} = 0 \tag{2}$$

$$\frac{D}{Dt}\mathbf{u} = -\nabla p + Pr\nabla^2\mathbf{u} + RaPrT\mathbf{y} \tag{3}$$

$$\frac{DT}{Dt} = \nabla^2 T \tag{4}$$

in terms of the Prandtl number $Pr = \nu/\alpha_T$ and the Rayleigh number $Ra = g\beta_T\Delta T d^3/\nu\alpha_T$. The boundary condition for $\mathbf{u}$ is the no-slip requirement. For T, the Neuman conditions $\partial T/\partial n = -q$ at $y = \pm 1/2$, and 0 or 1 at the vertical boundaries apply.

3. Base flow

Under the parallel flow assumption, namely, that $u = u(y)$ only, it is straightforward to introduce a stream function $\psi(y)$ so that the continuity equation (2) is automatically satisfied. The 2-D numerical solutions of Eqs. (2)–(4) shown in Fig. 2 reveal that such fully developed conditions are possible in the central area of the cavity, with streamlines nearly parallel with the x axis, provided that the value of the aspect ratio a is sufficiently large as we will discuss in the Results.

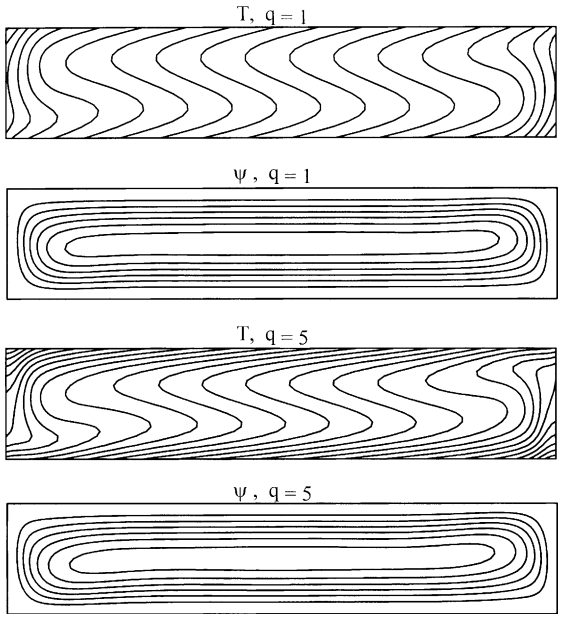

Fig. 2. Simulation with a 125 by 25 mesh of flow in a finite cavity, $Ra = 10^4$, $Pr = 0.7$ and $a = 5$.

Nevertheless, as long as the approximation is valid, it is not difficult [13] to show from Eqs. (3) and (4) that $T = \alpha x + \theta(y)$, up to an additive constant, so that the momentum and temperature equations finally reduce to

$$\begin{aligned} \psi'''' - \alpha Ra &= 0 \\ \theta'' - \alpha\psi' &= 0 \end{aligned} \tag{5}$$

with boundary conditions $\psi = \psi' = 0$ and $\theta' = -q$ at $y = \pm 1/2$, where the prime denotes differentiation with respect to y.

Solving Eq. (5) above in the coordinate system of Fig. 1 yields a solution of the form

$$\begin{aligned} \psi(y) &= \frac{\alpha Ra}{4!}\left(y^2 - \frac{1}{4}\right)^2 \\ T &= \alpha x - qy + \frac{\alpha^2 Ra}{4!}\left(\frac{y^5}{5} - \frac{y^3}{6} + \frac{y}{16}\right) \end{aligned} \tag{6}$$

for the base flow. For the crossed flux heating conditions considered here, the dimensionless temperature gradient α cannot be specified a priori. For given values of Ra and q, this parameter is determined instead from the integration of the temperature equation (4) in conservative form over an arbitrary section of the cavity. With the help of the divergence theorem, it follows next from the thermal energy balance and the boundary condition $\partial T/\partial x = 1$ on the side walls that

$$\int_{-1/2}^{1/2}\left(\psi' T + \frac{\partial T}{\partial x}\right)dy = -1 \tag{7}$$

The left-hand side of Eq. (7) may then be evaluated using Eq. (6) to obtain for the temperature gradient α the cubic equation

$$\frac{\alpha^3 Ra^2}{9!} + \alpha\left(1 - \frac{qRa}{6!}\right) - 1 = 0 \tag{8}$$

with one positive and two negative roots. Only the positive root, associated with the natural circulation pattern, will be considered for the purpose of deriving the stability equations.

4. Stability analysis

Let us introduce in the base flow small amplitude perturbations of the temperature, pressure, and velocity field components, propagating at some angle β with respect to the $(x–y)$ plane of Fig. 1. The next step is to assume an expansion of the form $f = f_0 + \varepsilon f_1 + \varepsilon^2 f_2 + \cdots$, in which ε is a formal parameter, for all variables in the set of governing equations (2)–(4). Multiple time scales $t_0 = t,\ t_1 = \varepsilon t,\ t_2 = \varepsilon^2 t, \ldots$ are also defined so that the nth-order equation system is

$$\begin{aligned}
&\nabla \cdot \mathbf{u}_n = 0\\
&\sum_{m=0}^{n} \frac{\partial \mathbf{u}_{n-m}}{\partial t_m} + (\mathbf{u}_m \cdot \nabla)\mathbf{u}_{n-m} = -\nabla p_n + Pr\nabla^2 \mathbf{u}_n + RaPrT_n\mathbf{y}\\
&\sum_{m=0}^{n} \frac{\partial T_{n-m}}{\partial t_m} + (\mathbf{u}_m \cdot \nabla)T_{n-m} = \nabla^2 T_n
\end{aligned} \tag{9}$$

with the original boundary conditions for $n = 0$ and their homogeneous counterparts when $n \geqslant 1$.

The solution at the order zero is simply the base flow solution, Eq. (6). The first-order solution is that of linear stability analysis. Let the vector $\hat{\mathbf{U}}_1 = (\hat{u}_1, \hat{v}_1, \hat{w}_1, \hat{p}_1, \hat{T}_1)^{\mathrm{T}}$ represent all first-order variables. We shall assume a separable first-order solution of the form $\mathbf{U}_1 = A(t)\hat{\mathbf{U}}_1(y)\exp(\mathrm{i}\tilde{\mathbf{k}} \cdot \mathbf{r})$ plus its complex conjugate (C.C.). Here $\tilde{\mathbf{k}} = k\mathbf{x} + l\mathbf{z}$ is the wavenumber vector, with a transverse component k and a longitudinal component l. These wavenumbers are assumed real, as it is customary for temporal stability analysis. Substituting the solution form of $\mathbf{U}_1$ into Eq. (9) for $n = 1$, it is found that the variables are separable only if

$$A(t) = \tilde{A}(t_1, t_2 \ldots)\mathrm{e}^{\sigma t_0} \tag{10}$$

where A, $\tilde{A}$ and $\sigma = \sigma_{\mathrm{r}} + \mathrm{i}\sigma_{\mathrm{i}}$ are complex quantities. The corresponding one-dimensional system in y with homogeneous boundary conditions $\hat{u} = \hat{v} = \hat{v}' = \hat{w} = \hat{T}' = 0$ at $y = \pm 1/2$ is then

$$\begin{bmatrix}
\mathrm{i}k & D & \mathrm{i}l & 0 & 0\\
PrL - \mathrm{i}k\psi' - \sigma & -\psi'' & 0 & -\mathrm{i}k & 0\\
0 & PrL - \mathrm{i}k\psi' - \sigma & 0 & -D & RaPr\\
0 & 0 & PrL - \mathrm{i}k\psi' - \sigma & -\mathrm{i}l & 0\\
-\alpha & -\theta' & 0 & 0 & L - \mathrm{i}k\psi' - \sigma
\end{bmatrix}
\begin{Bmatrix} \hat{u}_1\\ \hat{v}_1\\ \hat{w}_1\\ \hat{p}_1\\ \hat{T}_1 \end{Bmatrix} =
\begin{Bmatrix} 0\\0\\0\\0\\0 \end{Bmatrix} \tag{11}$$

with $D = \mathrm{d}/\mathrm{d}y$, while L stands for the operator $D^2 - k^2 - l^2$. For a given set of parameter values Ra, Pr, q, k and l, Eq. (11) defines an eigenvalue problem in σ. It is possible to write Eq. (11) in compact form as $\mathbf{L}(\tilde{\mathbf{k}}, \sigma)\hat{\mathbf{U}}_1 = \mathbf{0}$. One can equivalently split the operator $\mathbf{L}$ in two parts, namely as $\mathbf{L}(\tilde{\mathbf{k}}, \sigma) = \mathbf{A}(\tilde{\mathbf{k}}) - \sigma\mathbf{B}$, where the elements of matrix $\mathbf{B}$ are equal to either 0 or 1. To the eigenvalue problem above corresponds an adjoint problem $\mathbf{L}^{\dagger}\mathbf{U}_1^{\dagger} = \mathbf{0}$. The boundary conditions at $y = \pm 1/2$ for the adjoint problem are $v^{\dagger} = w^{\dagger} = Dw^{\dagger} = p^{\dagger} = DT^{\dagger} = 0$. The adjoint operator $\mathbf{L}^{\dagger} = (\mathbf{L}^*)^{\mathrm{T}}$ with $D \to -D$ is required by definition to satisfy the fundamental relationship

$$\langle \mathbf{Lf} | \mathbf{g} \rangle = \langle \mathbf{f} | \mathbf{L}^{\dagger}\mathbf{g} \rangle \tag{12}$$

for any pair of vectors $\mathbf{f}$ and $\mathbf{g}$. The inner product in Eq. (12) above is defined as

$$\langle \mathbf{f} | \mathbf{g} \rangle \stackrel{\Delta}{=} \sum_{i=1}^{5} \int_{-1/2}^{1/2} f_i^*(y) g_i(y)\,\mathrm{d}y \tag{13}$$

Unfortunately, unless $\alpha = 0$, Squire's theorem (see, for instance, Drazin and Reid [14]) cannot be used here to formally reduce the three-dimensional stability problem to an equivalent two-dimensional one. We must deal therefore with the full three-dimensional stability problem. But the eigenvalue problem Eq. (11) involves the singular matrix $\mathbf{B}$. The problem therefore is not in standard form as stated and must be rearranged prior to numerical solution. Fortunately, this can be done easily. We can choose for instance to eliminate $\hat{p}$ and $\hat{w}$ from Eq. (11), using the continuity and transverse momentum equations. We obtain as a result the reduced system of equations

$$\begin{bmatrix} -\tilde{k}^2(PrL-\mathrm{i}k\psi') & \mathrm{i}k(PrL-\mathrm{i}k\psi')D+l^2\psi'' & 0 \\ 0 & PrL^2-\mathrm{i}k(\psi' L-\psi''') & -\tilde{k}^2 RaPr \\ -\alpha & -\theta' & L-\mathrm{i}k\psi' \end{bmatrix} \begin{Bmatrix} \hat{u}_1 \\ \hat{v}_1 \\ \hat{T}_1 \end{Bmatrix} = \sigma \begin{bmatrix} -\tilde{k}^2 & \mathrm{i}kD & 0 \\ 0 & L & 0 \\ 0 & 0 & 1 \end{bmatrix} \begin{Bmatrix} \hat{u}_1 \\ \hat{v}_1 \\ \hat{T}_1 \end{Bmatrix} \tag{14}$$

defining the eigenvalue problem in standard form this time, where $\tilde{k}^2 = k^2 + l^2$ is simply the modulus of the wavenumber vector. The same procedure can be applied to the adjoint problem. Elimination of $u^\dagger$ and $p^\dagger$ from the original equation system leads to the equivalent problem

$$\begin{bmatrix} -(PrL+\mathrm{i}k\psi')D-2\mathrm{i}k\psi'' & \mathrm{i}k(PrL+\mathrm{i}k\psi') & \alpha D-\mathrm{i}k\theta' \\ \tilde{k}^2(PrL+\mathrm{i}k\psi') & -\mathrm{i}k(PrL+\mathrm{i}k\psi')D & -\alpha l^2 \\ 0 & RaPr & L+\mathrm{i}k\psi' \end{bmatrix} \begin{Bmatrix} v^\dagger \\ w^\dagger \\ T^\dagger \end{Bmatrix} = \sigma \begin{bmatrix} -D & \mathrm{i}k & 0 \\ \tilde{k}^2 & -\mathrm{i}kD & 0 \\ 0 & 0 & 1 \end{bmatrix} \begin{Bmatrix} v^\dagger \\ w^\dagger \\ T^\dagger \end{Bmatrix} \tag{15}$$

for the remaining adjoint variables.

4.1. Second order solution

Harmonic components of the basic perturbation are generated by the nonlinear terms of Eq. (9). A separable solution for $n = 2$ is assumed once again for all variables. Introducing the short-hand notation E for $\exp(\mathrm{i}kx + \mathrm{i}lz)$, the appropriate form of normal mode expansion of the second-order solution is now

$$\hat{\mathbf{U}}_2 = A_{20}(t)\hat{\mathbf{U}}_{20}(y) + A_{21}(t)\hat{\mathbf{U}}_{21}(y)E + \text{C.C.} + A_{22}(t)\hat{\mathbf{U}}_{22}(y)E^2 + \text{C.C.} + \cdots \tag{16}$$

It is found from Eq. (9) and (16), based on the orthogonality property of the powers of E, that the solution at the order E^0 is separable only if $A_{20} = |A|^2$. The corresponding one-dimensional system in terms of y is

$$\mathbf{L}(\mathbf{0}, 2\sigma_\mathrm{r})\hat{\mathbf{U}}_{20} = H_{-\tilde{\mathbf{k}},1}\mathbf{B}\hat{\mathbf{U}}_1^* + \text{C.C.} \tag{17}$$

The operator $H_{\pm\tilde{\mathbf{k}},1} \triangleq \pm\mathrm{i}k\hat{u}_1 + \hat{v}_1 D \pm \mathrm{i}l\hat{w}_1$ on the right-hand side of Eq. (17) acts on each component of the vector $\mathbf{B}\hat{\mathbf{U}}_1^*$. This equation has a purely real solution, in which $\hat{u}_{20}$ vanishes, provided that $\sigma(\mathbf{0}) \neq 2\sigma_\mathrm{r}(\tilde{\mathbf{k}})$. We assume that this is the case.

Repeating the procedure at the order E^1, one finds that $\hat{\mathbf{U}}_{21}$ is proportional to $\hat{\mathbf{U}}_1$. Since both solutions can be lumped together, it can be assumed without loss of generality that $\hat{\mathbf{U}}_{21}$ is equal to zero. At the order E^2 this time, separation of variables requires that $A_{22} = A^2$. The corresponding system in y is then

$$\mathbf{L}(2\tilde{\mathbf{k}}, 2\sigma)\hat{\mathbf{U}}_{22} = H_{\tilde{\mathbf{k}},1}\mathbf{B}\hat{\mathbf{U}}_1 \tag{18}$$

We take for granted here also that the condition $\sigma(2\tilde{\mathbf{k}}) \neq 2\sigma(\tilde{\mathbf{k}})$ for the existence of a solution is satisfied. At higher orders E^n, $n \geqslant 3$, homogeneous systems for $\hat{\mathbf{U}}_{2n}$ are found which only have the trivial solution. The complete second-order solution is then

$$\mathbf{U}_2 = |A|^2\hat{\mathbf{U}}_{20}(y) + A^2\hat{\mathbf{U}}_{22}(y)E^2 + A^{*2}\hat{\mathbf{U}}_{22}^*(y)E^{-2} \tag{19}$$

4.2. Third order solution

This solution is interesting mainly at the order E, since it allows the determination of the Landau coefficient. One more expansion of the third-order solution in powers of E

$$\mathbf{U}_3 = A_{30}(t)\hat{\mathbf{U}}_{30}(y) + A_{31}(t)\hat{\mathbf{U}}_{31}(y)E + \text{C.C.} + A_{32}(t)\hat{\mathbf{U}}_{32}(y)E^2 + \text{C.C.} + \cdots \tag{20}$$

together with Eq. (9) yields a system of one dimensional equations in y for each component of $\hat{\mathbf{U}}_{3n}$. Non homogeneous systems are found only for $\hat{\mathbf{U}}_{31}$ and $\hat{\mathbf{U}}_{33}$ however, leading to a solution in terms of E, E^3 and their complex conjugates exclusively. At the order E, separation of variables requires that $A_{31} = A|\overline{A}|^2$ and also that

$$\frac{\partial A}{\partial t_2} = KA|A|^2 \tag{21}$$

In Eq. (21), K is the complex Landau coefficient, to be determined as part of the solution of the one-dimensional system for $\hat{\mathbf{U}}_{31}(y)$

$$\mathbf{L}(\tilde{\mathbf{k}}, \sigma + 2\sigma_\mathrm{r})\hat{\mathbf{U}}_{31} = K\mathbf{B}\hat{\mathbf{U}}_1 + \hat{v}_1 D\mathbf{B}\hat{\mathbf{U}}_{20} + H^*_{-2\tilde{\mathbf{k}},1}\mathbf{B}\hat{\mathbf{U}}_{22} + H_{\tilde{\mathbf{k}},20}\mathbf{B}\hat{\mathbf{U}}_1 + H_{-\tilde{\mathbf{k}},22}\mathbf{B}\hat{\mathbf{U}}_1^* \tag{22}$$

Closer examination reveals that Eq. (22) is solvable as long as K is such that the solvability condition below is satisfied. Forming the inner product of Eq. (22) above with $\mathbf{U}_1^\dagger$ and using linearity gives

$$\left\langle \mathbf{L}(\tilde{\mathbf{k}}, \sigma)\hat{\mathbf{U}}_{31} | \mathbf{U}_1^\dagger \right\rangle = 2\sigma_\mathrm{r}\left\langle \mathbf{B}\hat{\mathbf{U}}_{31} | \mathbf{U}_1^\dagger \right\rangle + K^*\left\langle \mathbf{B}\hat{\mathbf{U}}_1 | \hat{\mathbf{U}}_1 \right\rangle + \left\langle \mathbf{g}_{31} | \mathbf{U}_1^\dagger \right\rangle \tag{23}$$

where $\mathbf{g}_{31}$ represents all the remaining terms on the right-hand side of Eq. (22). Since the left-hand side of Eq. (23) vanishes as a consequence of Eq. (12) and the definition of the adjoint solution, the solvability condition is therefore

$$\lim_{\sigma_\mathrm{r}\to 0} K^* = -\frac{\langle \mathbf{g}_{31} | \mathbf{U}_1^\dagger \rangle}{\langle \mathbf{B}\hat{\mathbf{U}}_1 | \mathbf{U}_1^\dagger \rangle} \tag{24}$$

setting at the same time the value of the Landau coefficient. Considering the multiple time scales defined earlier, the rate of change of A is given up to the second order in ε by

$$\frac{dA}{dt} = \frac{\partial A}{\partial t_0} + \varepsilon^2 \frac{\partial A}{\partial t_2} + \cdots = \sigma A + \varepsilon^2 K A |A|^2 + \cdots \tag{25}$$

Since ε is arbitrary, one can always redefine the product $\varepsilon A \to A$ in order to get the final form

$$\frac{dA}{dt} = \sigma A + K A |A|^2 + \cdots \tag{26}$$

Taking the real and imaginary parts of Eq. (26), it is easily found that the equilibrium solution for the modulus of A is $|A|_e = (-\sigma_r/K_r)^{1/2}$, provided that σ_r and K_r are of different signs. When the equilibrium solution exists, the bifurcation is classified as supercritical for $\sigma_r > 0$ and subcritical for $\sigma_r < 0$.

4.3. Bimodal stability

Transition between different types of instabilities occurs when the two instability modes share the same critical Rayleigh number at some q for a given Pr. This situation corresponds to a point of intersection of two marginal stability curves in a (Pr, Ra) or (q, Ra) plane, known as a codimension point [15]. Near a codimension point, located at a specific value of the Prandtl number $Pr_{cod}(q)$ for a given q, the simultaneous presence of two critical disturbance modes of different wavenumbers and amplitudes is possible. For instance, the interaction of stationary and oscillating modes, or oscillating thermal and hydrodynamic modes might occur. The previous unimodal analysis must then be generalized. The first-order bimodal solution is obtained by superposition of the solutions of Eq. (14) for each individual mode. The normal mode expansion in powers of E_H and E_T of the second-order solution is then

$$\begin{aligned}\mathbf{U}_2 = {} & |A_H|^2 \hat{\mathbf{U}}_{20H}(y) + |A_T|^2 \hat{\mathbf{U}}_{20T}(y) + A_H^2 \hat{\mathbf{U}}_{22H}(y) E_H^2 \\ & + A_T^2 \hat{\mathbf{U}}_{22T}(y) E_T^2 + A_H A_T \hat{\mathbf{U}}_{21H}(y) E_H E_T \\ & + A_H A_T^* \hat{\mathbf{U}}_{21T}(y) E_H E_T^{-1} + \text{C.C.}\end{aligned} \tag{27}$$

The subscripts H and T are used to indicate the terms associated with each mode, the hydrodynamic or the thermal for instance. The first four terms on the right-hand side of Eq. (27) correspond to the second-order solutions for the uncoupled modes. The remaining terms are the result of mode coupling. They are found by solving their corresponding one-dimensional equations in y

$$\begin{aligned}\mathbf{L}(\tilde{\mathbf{k}}_H + \tilde{\mathbf{k}}_T, \sigma_H + \sigma_T)\hat{\mathbf{U}}_{21H} &= H_{\tilde{\mathbf{k}}_T,1H}\mathbf{B}\hat{\mathbf{U}}_{1T} \\ \mathbf{L}(\tilde{\mathbf{k}}_H - \tilde{\mathbf{k}}_T, \sigma_H + \sigma_T^*)\hat{\mathbf{U}}_{21T} &= H_{-\tilde{\mathbf{k}}_T,1H}\mathbf{B}\hat{\mathbf{U}}_{1T}^*\end{aligned} \tag{28}$$

Repeating the expansion procedure for the third-order solution, it turns out that separation of variables is possible as before if, first, the solution at the order E_H, E_T is of the form

$$\begin{aligned}\mathbf{U}_{31} = {} & [A_H|A_H|^2 \hat{\mathbf{U}}_{31H}^H(y) + A_H|A_T|^2 \hat{\mathbf{U}}_{31H}^T(y)]E_H \\ & + [A_T|A_H|^2 \hat{\mathbf{U}}_{31T}^H(y) + A_T|A_T|^2 \hat{\mathbf{U}}_{31T}^T(y)]E_T + \text{C.C.}\end{aligned} \tag{29}$$

and, second, the amplitudes are interrelated as follows

$$\begin{aligned}\frac{\partial A_H}{\partial t_2} &= K_{HH} A_H |A_H|^2 + K_{HT} A_H |A_T|^2 \\ \frac{\partial A_T}{\partial t_2} &= K_{TH} A_T |A_H|^2 + K_{TT} A_T |A_T|^2\end{aligned} \tag{30}$$

Thus, the rate of change of the amplitudes involves four Landau coefficients. The coefficients K_{HH} and K_{TT} are the coefficients for the uncoupled modes. They are found from the first-order and adjoint solutions of each respective mode, using Eq. (24). The other coefficients can be determined from the solvability condition of

$$\begin{aligned}\mathbf{L}(\tilde{\mathbf{k}}_H, \sigma_H + 2\sigma_{rT})\hat{\mathbf{U}}_{31H}^T &= K_{HT}\hat{\mathbf{U}}_{1H} + \mathbf{g}_{31H}^T \\ \mathbf{L}(\tilde{\mathbf{k}}_T, \sigma_T + 2\sigma_{rH})\hat{\mathbf{U}}_{31T}^H &= K_{TH}\hat{\mathbf{U}}_{1T} + \mathbf{g}_{31T}^H\end{aligned} \tag{31}$$

The adjoint solutions $\mathbf{U}_H^\dagger$, $\mathbf{U}_T^\dagger$ are required to form the inner product with the first and second equation in Eq. (31), respectively. The expressions for the terms $\mathbf{g}_{31H}^T$, $\mathbf{g}_{31T}^H$ above are rather lengthy, however. For this reason, they are left in Appendix. Once the Landau coefficients are known, the bimodal equilibrium solution of Eq. (30) for the magnitude of A_H, and A_T is

$$\begin{aligned}|A_H|_e^2 &= \frac{\sigma_{rT}K_{rHT} - \sigma_{rH}K_{rTT}}{K_{rHH}K_{rTT} - K_{rHT}K_{rTH}} \\ |A_T|_e^2 &= \frac{\sigma_{rH}K_{rTH} - \sigma_{rT}K_{rHH}}{K_{rHH}K_{rTT} - K_{rHT}K_{rTH}}\end{aligned} \tag{32}$$

Suslov and Paolucci [16] analysed the solution Eq. (32) and concluded that it is stable only if $K_{rHT}K_{rTH} < 0$ and $C_{HH} + C_{TT} < 0$, where

$$\begin{aligned}C_{HH} &= \sigma_{rH} + 3|A_H|_e^2 K_{rHH} + |A_T|_e^2 K_{rHT} \\ C_{TT} &= \sigma_{rT} + |A_H|_e^2 K_{rTH} + 3|A_T|_e^2 K_{rTT}\end{aligned} \tag{33}$$

The reduced eigenvalue problem Eq. (14) is readily solvable by classical numerical methods. One of the most straightforward is to solve the equations by finite-differences. Five-point central shemes are used thoroughout, allowing fourth-order accuracy for the first and second derivatives and second-order accuracy for the higher derivatives. The homogeneous Neuman boundary conditions of Eq. (14) are also discretized using forward and backward fourth-order difference formulas. The adjoint problem Eq. (15) is treated similarly.

The eigenvalues of the discrete system matrices are computed using the DGVLCG subroutine from the IMSL library. For N computational points, the value of Ra for which the maximal growth rate σ_r among the $3N$ eigenvalues cancels is determined iteratively by Newton's method, holding q, k, l, Pr constant. A

marginal stability surface for given values of q ranging from 0.5 to 8 and Pr ranging from 0.25 to 100 is generated by repeating the procedure for different wavenumbers. The minimum value of Ra over the stability surface determines the critical Rayleigh number $Ra_c(q, Pr)$.

The five-point scheme is also used to perform the discretization of Eqs. (17), (18) and (28). Let us mention by the way that Eq. (18) is an ill-conditioned system. A solution for the non vanishing components of $\hat{\mathbf{U}}_{20}$ is then better found by least squares using the DLSBRR routine. All the other equations are solved directly with the DLSACG routine.

The unimodal stability results presented in the next section were computed using $N = 90$ grid points. The finite difference code was validated by the duplication of Bergholz's results. A very good overall agreement between both sets of predictions was found [13], over the range of Pr values and stratification levels considered, if we used $N = 80$ or 100. Finer meshes are required for bimodal stability however. The amplitude plot in Fig. 12 needed $N = 150$ to ensure reasonable grid independence.

5. Results

To begin with, the full set of governing equations Eqs. (2)–(4), is solved numerically with a different code in a finite width cavity in two dimensions in order to test the validity of the parallel flow approximation. Calculations are performed for different values of q at $Ra = 10^4$ and $Pr = 0.7$, based on fully implicit time discretization, with spatial discretization by control volumes using the power-law scheme of Patankar [17].

The maximum value of the numerical solution for Ψ is plotted versus the cavity aspect ratio a in Fig. 3 for $Ra = 10^4$ and $Pr = 0.7$. Comparison with the parallel flow solution value obtained from Eq. (6), which is strictly valid only for a cavity extending to infinity along x, reveals very good agreement between the solutions for $a \geqslant 4$ or so when $q = 1$. Aspect ratios of the order of 7 are required for $q = 5$. For larger heat flux ratios q, it seems reasonable then to expect that larger aspect ratios are required before it is safe to make the parallel flow approximation. Thus, the validity of the parallel approximation for the base flow over the central region of the cavity is confirmed for small values of q. Further experimentations reveal that parallel flow is estabished very early in the cavity, in fact as soon as $Ra = \mathcal{O}(10^3)$. Thus, a and q are the main parameters to select in order to obtain parallel flow in the enclosure.

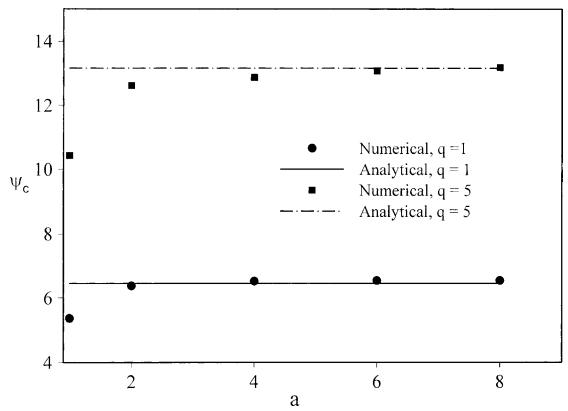

Fig. 3. Streamfunction maximum versus a for $Pr = 0.7$, $q = 1, 5$.

Preliminary investigations of the solutions of the eigenvalue problem Eq. (14) reveal that two-dimensional transverse disturbances (propagating along the x-direction) are not critical at any Prandtl number considered in this study. The critical disturbances are propagating at a large angle β in the $(x–z)$ plane and always involve the three velocity components. The angle β defines the direction of propagation in such a way that $k = \tilde{k}\cos\beta$ and $l = \tilde{k}\sin\beta$. It is used simply because the discussion of the stability results is easier to follow in terms of $\tilde{k}$ and β rather than in k and l.

It is well established in stability theory that the physical origin of the disturbances is different depending on the value of Pr. Either hydrodynamic modes, owing to a destabilization of the base flow velocity, or thermal modes, generated by destabilization of the temperature will occur first. If $Pr < 1$, the fluid thermal diffusivity is greater than its viscous diffusivity. Thermal disturbances of the base flow are then prone to be dissipated faster than hydrodynamic disturbances, and instabilities most likely to be caused by hydrodynamic disturbances, gaining energy from the base flow by the action of shear. On the other hand, as Pr increases, thermal, buoyancy-driven disturbances are expected to be at the origin of the main mode of instabilities.

Solution of the eigenvalue problem Eq. (14) also reveal that σ_i is not equal to zero at the critical Rayleigh when the Prandtl number is small, indicating an oscillating instability of the base flow solution, while there are no oscillations for larger Pr. Steady and oscillating instabilities were similarly reported by Bergholz [11] in the case of a vertical cavity with a fixed temperature difference imposed between the walls. But the finding is in contrast with the case of a porous layer heated from a single flux [9], where instabilities are always oscillating.

Fig. 4 displays the marginal stability curves for the critical longitudinal disturbances propagating along $\beta_c = \pi/2$ for $q = 1$ and different values of Pr. Each curve has two branches, associated with the hydrodynamic oscillating mode and the thermal steady mode, respectively, as discussed below. It appears that the stability curve for $Pr = 1$ has only one minimum at large wavenumber $\tilde{k}$. The curve for $Pr = 0.7$ on the other hand

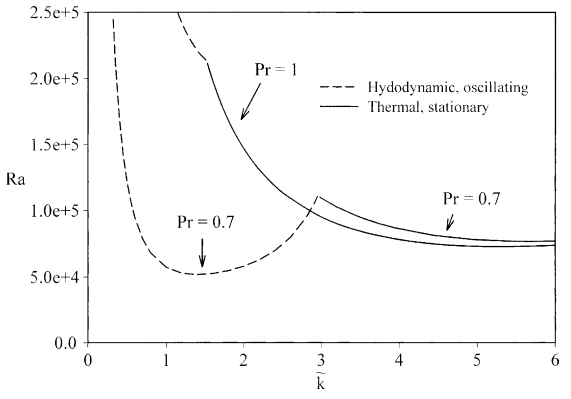

Fig. 4. Marginal stability at $\beta = \pi/2$ for $q = 1$, $Pr = 0.7$, 1.

displays not one, but two minima at a small and a large wavenumber. Each minimum indicates the Rayleigh number for the onset of the thermal and the hydrodynamic mode, with the hydrodynamic mode as the critical one in the present case. We were able to detect in a cavity of aspect ratio $a = 6.2$ small amplitude oscillations with a frequency $\omega \approx 100$ of the maximum ψ value of the numerical solution of Eqs. (2)–(4) for $Ra = 1.175 \times 10^5$, $q = 1$, $Pr = 0.7$ with the computer code used to simulate the base flow. This value, obtained from a 125 by 25 mesh and a time step $\Delta t = 5 \times 10^{-4}$, is reasonably close to the theoretical value $\omega = 90.98$.

Fig. 5 shows the critical Rayleigh number Ra_c versus the Prandtl number for different values of q. The critical direction $\beta_c = \pi/2$ is the same for the entire range of Pr and q considered. That is, the critical disturbances are always propagating along z. Computation of the Landau coefficient reveals that the bifurcation is supercritical in all cases, with a stable equilibrium solution for the amplitude A of the disturbance when $Ra/Ra_c > 1$. It is clear from the plots that the value of Ra_c for the hydrodynamic mode is strongly dependent upon the value of Pr. For the thermal mode however, the influence of Pr is far less pronounced and rapidly becomes negligible as Pr increases beyond 4 or 5. It is seen also that the base flow is much more stable for Prandtl numbers slightly above, say, one than for smaller Pr values. Some caution is necessary with the results, as the parallel approximation might break down in a cavity of finite extent when Ra is too small. Numerical simulations with $q = 5$, $Pr = 0.3$, is n a finite cavity with aspect ratio $a = 5$ reveal that the flow is not truly parallel at $Ra = 500$ for instance. Predictions of Ra_c of this order of magnitude therefore, corresponding to the smallest Pr values, should be regarded as asymptotic results having only indicative value. The heat flux ratio also plays an important role. The influence of the parameter q in the determination of Ra_c is significant. When $q < 1$, Ra_c increases steeply because instabilities only happen at very large Rayleigh numbers for a cavity heated sideways, i.e. for $q = 0$. It is found from Fig. 5, not surprisingly, that increasing the flux ratio q reduces the value of Ra_c, as heating the fluid from below is destabilizing.

Fig. 6 describes the variation of the critical wavenumber k_c with Pr. There is a discontinuous transition from the low wavenumbers of the hydrodynamic mode to the high wavenumbers of the thermal mode, at the value of Pr corresponding to the codimension point Pr_{cod} for each value of q considered. The case of $q = 1$ is instructive. Besides the critical modes along $\beta_c = \pi/2$, indicated by solid lines on Fig. 6, with transition between hydrodynamic and thermal modes at $Pr_{cod} = 0.764$, there exists for $q \leqslant 1$ a second branch of oblique hydrodynamic modes with $\beta_c < \pi/2$. This second branch is shown for $q = 1$ on the figure, where it extends over the range $0.651 < Pr < 0.856$. Computation of the Landau coefficient reveals that the bifurcation is subcritical on this branch. There is then no equilibrium solution for the disturbance amplitude A when $Ra/Ra_c > 1$ and no stable

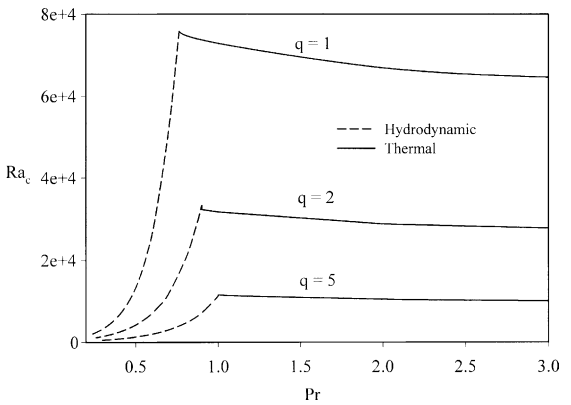

Fig. 5. Critical Rayleigh number versus Pr, $q = 1$, 2, 5.

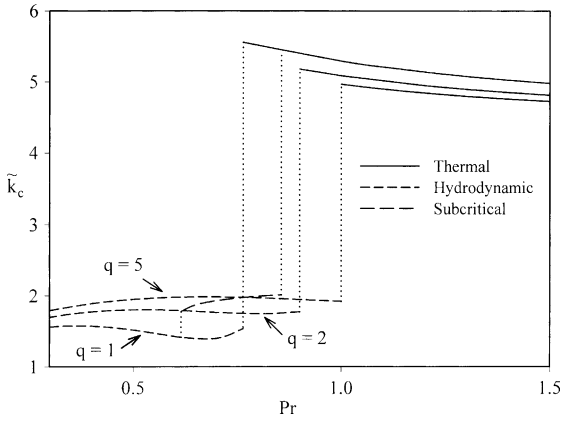

Fig. 6. Critical wavenumber vector modulus $\tilde{k}_c$ versus Pr, $q = 1$, 2, 5.

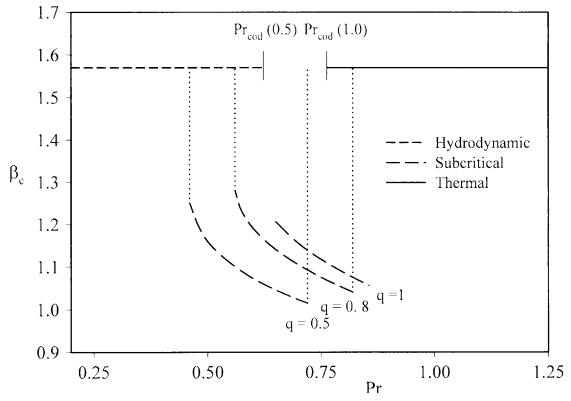

Fig. 7. Critical direction of propagation β_c versus Pr, $q = 0.5$, 0.8, 1.

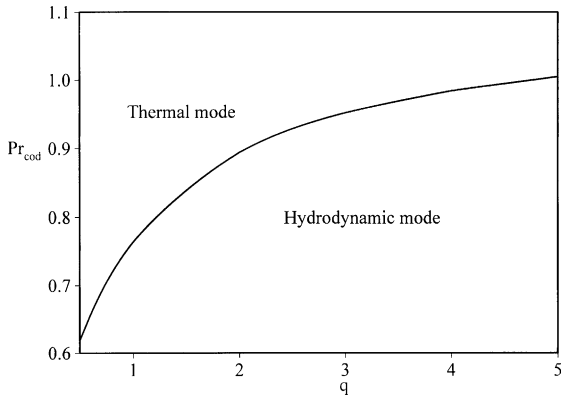

Fig. 9. Prandtl number value at codimension point versus q.

solution other than zero when $Ra/Ra_c < 1$. One can further notice that smaller values of k_c for the thermal mode are found for larger values of q, while it is just the opposite for the hydrodynamic mode.

Fig. 7 shows the direction of propagation β_c of the critical disturbance versus Pr for $q = 0.5$, 0.8 and 1. It is clear from the plot that the direction $\beta_c = \pi/2$ is unaffected by the value of Pr for the stable supercritical critical branch of the hydrodynamic mode and the thermal mode. The transition from one mode to the other occurs at a value of Pr_{cod} of 0.619 and 0.764 for $q = 0.5$ and 1, respectively. For the subcritical branches of the hydrodynamic mode however, the angle β_c decreases smoothly with Pr. For the sake of completeness, the oscillation frequency $\omega_c = \sigma_i$ is shown versus Pr in Fig. 8 for $q = 1$, 2, 5. The frequency of the hydrodynamic instability cells appears to be increasing steadily with Pr in all cases. The value of ω_c abruptly drops to zero for $Pr > Pr_{cod}$ where transition to the steady thermal mode occurs.

The codimension points naturally define a curve $Pr_{cod}(q)$ representing the borderline between the thermal and hydrodynamic modes as depicted in Fig. 9, summarizing what type of instability will occur for given values of the parameters q and Pr according to the linear stability theory. The Rayleigh number at the codimension point is found to decrease steadily with q, as expected, from a value of $Ra_c = 7.579 \times 10^4$ when $q = 1$ to a value of $Ra_c = 1.149 \times 10^4$ when $q = 5$. The computations also reveal that hydrodynamic instabilities can occur for Pr values slightly greater than 1.0 if q is larger than 5.0 or so.

The kinetic and thermal potential energy balances of the disturbances can give us some insight in connection with the physical mechanisms driving the instability modes. Multiplying Eq. (11) by the complex conjugate of $\mathbf{B}\hat{\mathbf{U}}_1$, integrating over $[-1/2, 1/2]$ with respect to y and taking the real part of the results gives, after a few rearrangements

$$\begin{aligned} \sigma_r E_{kin} &= -Pr\dot{E}_{vis} + \dot{E}_U + RaPr\dot{E}_B \\ \sigma_r E_{pot} &= -\dot{E}_{dif} + \dot{E}_T + \alpha\dot{E}_S \end{aligned} \tag{34}$$

for the rates of change of the disturbance kinetic energy E_{kin} and thermal potential energy E_{pot}. Each term

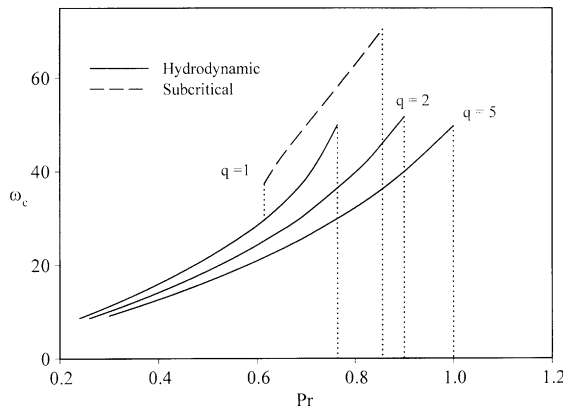

Fig. 8. Critical oscillation frequency ω_c versus Pr, $q = 1$, 2, 5.

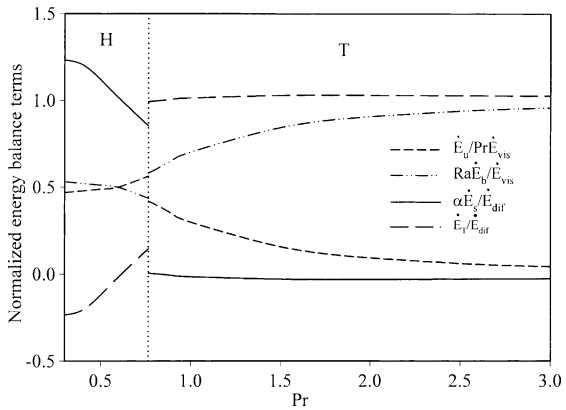

Fig. 10. Disturbance energy balance versus Pr, $q = 1$.

appearing in Eq. (34) is defined in appendix. Their meaning is as follows. First, $-Pr\dot{E}_{vis}$ and $-\dot{E}_{dif}$ are always negative and account for the rate of kinetic energy loss due to viscous dissipation and potential energy loss due to heat diffusion, respectively. Among the remaining terms, $\dot{E}_U$ is the rate of kinetic energy transfer from the base flow, $RaPr\dot{E}_B$ is the rate of change of kinetic energy caused by buoyancy, while $\alpha\dot{E}_S$ represents the rate of change of potential energy related to stratification. Finally, $\dot{E}_T$ is the rate of change of potential energy associated with the interactions of the disturbance with the vertical temperature gradient.

The relative values of the energy balance terms in Eq. (34) are displayed versus Pr in Fig. 10 at the critical Rayleigh number for $q = 1$. Normalization of the data, is done with respect to $-Pr\dot{E}_{vis} = -1$ and $-\dot{E}_{dif} = -1$, in such a way that the sum of the normalized $\dot{E}_U$ and $RaPr\dot{E}_B$ values, as well as that of $\alpha\dot{E}_S$ and $\dot{E}_T$, should be equal to one in principle on the graph. The transition between modes at Pr_{cod} is associated with a net discontinuity in all the profiles. The plots reveal that for $Pr < 0.764$, the kinetic energy of the disturbance comes nearly equally from the shear and buoyancy terms. The instability is then hydrodynamic. For $Pr > 0.764$, the contribution of the shear term becomes rapidly negligible and the disturbance derives the bulk of its kinetic energy from the buoyancy term. The instability is then thermal.

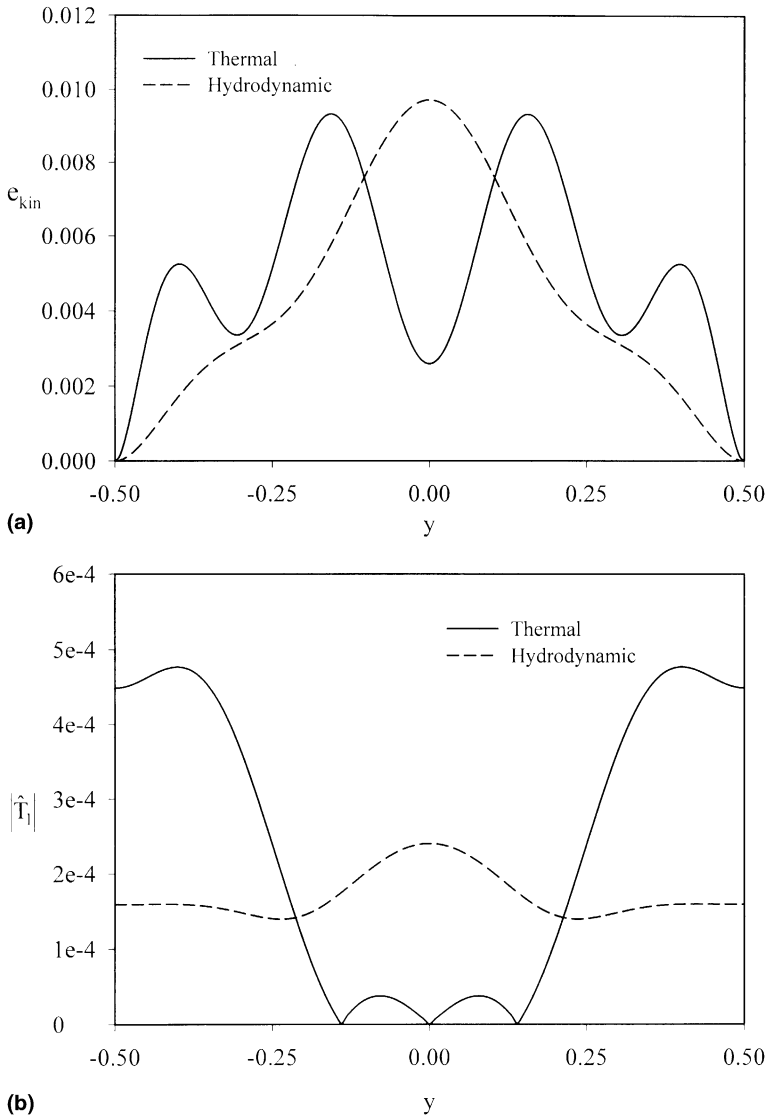

Fig. 11. (a) Disturbance kinetic energy per unit volume versus y, $Pr = 0.764$, $q = 1$. (b) Modulus of disturbance temperature versus y, $Pr = 0.764$, $q = 1$.

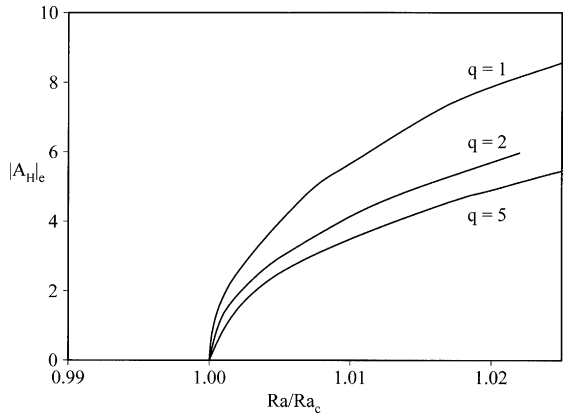

Fig. 12. Equilibrium amplitude versus *Ra*, hydrodynamic mode, $Pr = 0.764$, $q = 1$.

The sharp contrast in the form of the solutions $\hat{\mathbf{U}}_{1H}$ and $\hat{\mathbf{U}}_{1T}$ can be appreciated by considering the kinetic energy per unit volume of the disturbance

$$2e_{kin} = |\hat{u}_1|^2 + |\hat{v}_1|^2 + |\hat{w}_1|^2 \tag{35}$$

at Pr_{cod}. Fig. 11(a) shows the profile of e_{kin} versus y of the thermal and hydrodynamic solutions for $q = 1$ at the codimension point $Pr_{cod} = 0.764$. The hydrodynamic mode has its peak of local kinetic energy at the mid-plane $y = 0$ of the domain. The thermal mode on the other hand shows four energy peaks located symmetrically between the mid-plane and $y = \pm 0.5$. The modulus of the temperature component of the solution for each mode is plotted versus y in Fig. 11(b). The contrast between the two solutions is once again obvious. The amplitude gradients are very mild for the hydrodynamic mode, except perhaps near the center, and much more important for the thermal mode elsewhere.

Computation of the four Landau coefficients of Eq. (30) at the codimension point Pr_{cod} for $q = 1$, 2, 5 and Eq. (33) finally reveals that there can be no stable bimodal equilibrium solution Eq. (32) for the thermal and the hydrodynamic mode. Only one mode can be present at the codimension point therefore. Since the thermal mode turns out to be subcritical, it will be the hydrodynamic mode. Fig. 12 displays the equilibrium amplitude solution $|A_H|_e$ of Eq. (26) for the hydrodynamic mode at Pr_{cod} versus the ratio Ra/Ra_c for $q = 1$, 2, 5. The fact that no equilibrium solution exists for $Ra < Ra_c$, i.e. while σ_r is still negative, is a clear indication that the hydrodynamic mode corresponds to a supercritical bifurcation.

6. Conclusion

The multiple timescale, normal mode expansion shows that stable, supercritical bifurcations of the parallel base flow always occur for longitudinal disturbances involving three velocity components, for the range of parameters *Pr* and *q* considered in this study. Depending on the value of these parameters, the instability is either oscillating and shear-driven, for small *Pr*, or steady and buoyancy-driven for larger *Pr*. Thus, instabilities are not always oscillating, in contrast with what is found in the case of a porous layer heated from a single flux. There exists an unstable, subcritical branch of the hydrodynamic mode, for oblique disturbances when $q \leqslant 1$. Computations of the Landau coefficients for the two interacting modes reveal that the hydrodynamic mode is the only stable mode at the codimension points.

Acknowledgment

This research was supported by the Natural Sciences and Engineering Research Council of Canada.

Appendix A

The additional terms on the right-hand side of Eq. (31) respectively stand for

$$\mathbf{g}^{T}_{31H} = \hat{v}_{1H} D\mathbf{B}\hat{\mathbf{U}}_{20T} + H_{\tilde{\mathbf{k}}_H - \tilde{\mathbf{k}}_T, 1T}\mathbf{B}\hat{\mathbf{U}}_{21T} + H^{*}_{-\tilde{\mathbf{k}}_H - \tilde{\mathbf{k}}_T, 1T}\mathbf{B}\hat{\mathbf{U}}_{21H} + H_{\tilde{\mathbf{k}}_H, 20T}\mathbf{B}\hat{\mathbf{U}}_{1H} + H_{\tilde{\mathbf{k}}_T, 21T}\mathbf{B}\hat{\mathbf{U}}_{1T} + H_{-\tilde{\mathbf{k}}_T, 21H}\mathbf{B}\hat{\mathbf{U}}^{*}_{1T}$$

$$\mathbf{g}^{H}_{31T} = \hat{v}_{1T} D\mathbf{B}\hat{\mathbf{U}}_{20H} + H_{-\tilde{\mathbf{k}}_H + \tilde{\mathbf{k}}_T, 1H}\mathbf{B}\hat{\mathbf{U}}_{21H} + H^{*}_{-\tilde{\mathbf{k}}_H - \tilde{\mathbf{k}}_T, 1H}\mathbf{B}\hat{\mathbf{U}}_{21H} + H_{\tilde{\mathbf{k}}_T, 20H}\mathbf{B}\hat{\mathbf{U}}_{1T} + H^{*}_{-\tilde{\mathbf{k}}_H, 21T}\mathbf{B}\hat{\mathbf{U}}_{1H} + H_{-\tilde{\mathbf{k}}_H, 21H}\mathbf{B}\hat{\mathbf{U}}^{*}_{1H}$$

The various quantities appearing in the disturbance energy balances Eq. (34) are defined as follows

$$E_{kin} = \frac{1}{2}\int_{-1/2}^{1/2} e_{kin}\,dy$$

$$E_{pot} = \frac{1}{2}\int_{-1/2}^{1/2} |\hat{T}_1|^2\,dy$$

$$\dot{E}_{vis} = \frac{1}{2}\int_{-1/2}^{1/2} \tilde{k}^2(|\hat{u}_1|^2 + |\hat{v}_1|^2 + |\hat{w}_1|^2) + |\hat{u}'_1|^2 + |\hat{v}'_1|^2 + |\hat{w}'_1|^2\,dy$$

$$\dot{E}_{dif} = \frac{1}{2}\int_{-1/2}^{1/2} |\hat{T}'_1|^2 + \tilde{k}^2|\hat{T}_1|^2\,dy$$

$$\dot{E}_{U} = \frac{1}{2}\int_{-1/2}^{1/2} \psi'' Re(\hat{v}_1\hat{u}^{*}_1)\,dy$$

$$\dot{E}_{B} = \frac{1}{2}\int_{-1/2}^{1/2} Re(\hat{v}^{*}_1\hat{T}_1)\,dy$$

$$\dot{E}_T = -\frac{1}{2}\int_{-1/2}^{1/2} \theta' Re(\hat{v}_1 \hat{T}_1^*)\,dy$$

$$\dot{E}_S = -\frac{1}{2}\int_{-1/2}^{1/2} Re(\hat{u}_1 \hat{T}_1^*)\,dy$$

References

[1] D. Riley, K.H. Winters, Time periodic convection in porous media: the evolution of Hopf bifurcations with aspect ratios, J. Fluid Mech. 223 (1991) 457–474.

[2] H.D. Murphy, Convective instabilities in vertical fractures and faults, J. Geophys. Res. 84 (1979) 6121–6130.

[3] M. Wang, D.R. Kassoy, P.D. Weidman, Onset of convection in a vertical slab of porous media between two impermeable conducting blocks, Int. J. Heat Mass Transfer 30 (1987) 1331–1341.

[4] A. Bejan, The boundary layer regime in a porous layer with uniform heat flux from the side, Int. J. Heat Mass Transfer 26 (1983) 1339–1346.

[5] P. Vasseur, M.G. Satish, L. Robillard, Natural convection in a thin inclined porous layer exposed to a constant heat flux, Int. J. Heat Mass Transfer 30 (1987) 537–549.

[6] M. Sen, P. Vasseur, L. Robillard, Multiple steady states for unicellular natural convection in an inclined porous layer, Int. J. Heat Mass Transfer 30 (1987) 2097–2113.

[7] S. Kimura, I. Pop, Conjugate natural convection between concentric horizontal cylinders filled with a porous medium, Wärme und Stoffübertr. 27 (1992) 85–91.

[8] F.H. Bark, F. Alavyoon, A.A. Dahlkild, On unsteady free convection in vertical slots due to prescribed fluxes of heat and mass at the vertical walls, J. Fluid Mech. 235 (1992) 665–689.

[9] S. Kimura, M. Vynnycky, F. Alavyoon, Unicellular natural circulation in a shallow horizontal porous layer heated from below by a constant flux, J. Fluid Mech. 294 (1995) 231–257.

[10] D.A. Nield, Convection in a porous medium with inclined temperature gradient, Int. J. Heat Mass Transfer 34 (1991) 87–92.

[11] R.F. Bergholz, Instability of steady natural convection in a vertical fluid layer, J. Fluid Mech. 84 (1978) 743–768.

[12] D.D. Gray, A. Giorgini, The validity of the Boussinesq approximation for liquids and gases, Int. J. Heat Mass Transfer 19 (1976) 545–551.

[13] M. Prud'homme, H. Bougherara, A. Bahloul, Convection in a vertical cavity submitted to crossed uniform heat fluxes, Int. J. Heat Mass Transfer 46 (2003) 3831–3840.

[14] P.G. Drazin, W.H. Reid, Hydrodynamic Stability, Cambridge University Press, 1991.

[15] P. Chossat, G. Iooss, The Couette–Taylor Problem, Springer-Verlag, 1994.

[16] S.A. Suslov, S. Paolucci, Nonlinear analysis of convection flow in a tall vertical enclosure under non-Boussinesq conditions, J. Fluid Mech. 344 (1997) 1–41.

[17] S.V. Patankar, Numerical Heat Transfer and Fluid Flow, McGraw-Hill, 1980.